



Microwave assisted synthesis of porous carbon from graphene for enhanced adsorption of atrazine in aqueous solution

Xiuzhen Zhu^{a,b,*}, Hongliang Xu^a, Haiwen Xie^a, Guangcai Tan^a, Yue Gao^a, Nan Xu^a

^aKey Laboratory for Heavy Metal Pollution Control and Reutilization, School of Environment and Energy, Peking University Shenzhen Graduate School, Shenzhen 518055, China, Tel. 0755-88018736; emails: zhuxz@pkusz.edu.cn (X. Zhu), hongliangxu.pku@outlook.com (H. Xu), 1601214110@sz.pku.edu.cn (H. Xie), 1301213827@sz.pku.edu.cn (G. Tan), gaoyue@sz.pku.edu.cn (Y. Gao), xunan@pkusz.edu.cn (N. Xu)

^bDepartment of Chemistry, Southern University of Science and Technology, Shenzhen 518055, China

Received 5 September 2020; Accepted 22 August 2020

ABSTRACT

In order to improve the adsorption capacity of graphene oxide (GO), graphene-based porous carbon (GPC) was synthesized by a two-step activation method. Using chemical activation of microwave exfoliated GO, we obtained GPC with a high Brunauer–Emmett–Teller surface area of up to 1,598 m²/g and a large number of micropores. The GPC was firstly used as an adsorbent for the removal of atrazine in aqueous solution. The obtained adsorbent was characterized by scanning electron microscopy, BET, X-ray diffraction, Fourier transform infrared, and Raman spectroscopy. Experimental results indicated that GPC had excellent adsorption capacity (~131.6 mg/g), which was much higher than that of GO synthesized by the Hummer' method. The adsorption process was more accurately represented by a pseudo-second-order model and Freundlich isotherm model for the adsorption of atrazine on GPC. The present adsorption studies of pesticides revealed the potential of GPC nanomaterial to be utilized as a promising adsorbent for organic pollutants.

Keywords: Atrazine adsorption; Graphene; Porous carbon; Microwave; Water purification

1. Introduction

Nowadays, the contamination of water resources by a variety of pollutants from industrial production has been a global issue that threatens the health of humans and the function of ecosystem. Water purification is recognized as a top 21st century challenge [1]. Because of the extensive use of pesticides in industry and particularly in agriculture, more, and more water sources are contaminated with pesticides [2]. Atrazine, 2-chloro-4-ethylamino-6-isopropylamino-s-triazine, is one of the most widely applied herbicides due to its high efficiency [3]. Leaching and retention of atrazine in the field have led to the high potential of surface water and groundwater contamination. Acting as an endocrine-disrupting chemical (EDC), atrazine

can also affect central nervous, reproductive, and immune systems and poses potential risks to human health [4,5].

Adsorption is one of the most effective techniques that have been applied to remove contaminants because of its low cost and easy operation. Porous material including activation carbon [6–8], zeolites [9], and metal-organic frameworks (MOFs) [10–13] are all effective sorbents for pollutants removal due to their various chemical composition and structural architectures. Among this, porous carbonaceous materials are commonly used as efficient adsorbents because of their distinct advantages, which include a broad pore size distribution, high surface area, and large pore volume [14–20].

Graphene is a new carbon material possessing many unique features such as good electrical, thermal, and mechanical properties [21,22]. Graphene-based material

* Corresponding author.

derived from graphite oxide is now being manufactured in ton quantities at low cost [23], attracting broad research interest in environmental application [24–30]. However, GO normally prepared by modified Hummer' method or other methods exhibits much lower specific surface area values compared with the theoretical values predicted (2,630 m²/g), which results in the reduction of its adsorption capacity for the removal of pollutants and limitation of its application as adsorbents. In order to improve this disadvantage, several activation methods have been developed for increasing the specific surface area and adsorption capacity. In general, physical activation is performed in a CO₂ or hydrothermal steam atmosphere at a high temperature, and chemical activation can be achieved using different chemical reagents, typically KOH, NaHCO₃, or H₃PO₄ [28,31]. KOH activation has been extensively used on biochar, carbon nanotubes (CNTs), and carbon nanofibers to improve porosity [32]. Guo et al. [28] synthesized activated graphene adsorbents with a specific area of 512.6 m²/g by a one-step alkali-activated method. Tan et al. [32] reported KOH modified biochar and activated carbon with increased adsorption capacity using corn straw biochar as a precursor. As a convenient and rapid heating source, microwave irradiation has also been used for reduction of graphene oxide [33]. Zhu et al. [35] achieved the exfoliation and reduction of graphite oxide by treating graphite oxide powders in a commercial microwave oven [34]. However, few investigations have been reported on graphene-based porous carbon (GPC) prepared by combining physical and chemical activation process for pollutant adsorption.

Herein, we synthesized a GPC adsorbent with significantly improved adsorptive performance to pesticides. This work aims to: (i) prepare porous carbon adsorbent by microwave exfoliation and KOH activation of graphene oxide, (ii) investigate the adsorption behavior of atrazine by batch experiment, and (iii) discuss the kinetics, equilibrium modeling, environmental factors, and interaction mechanism of adsorption of atrazine. This study provides a novel and promising nanomaterial for environmental remediation.

2. Materials and experiment methods

2.1. Chemicals and materials

Atrazine was provided by Aldrich Chemical Co. (America) with a purity of >98%. Potassium hydroxide (KOH), sodium chloride (NaCl), sodium hydroxide (NaOH), and hydrochloric acid (HCl) were purchased from Sinopharm Chemical Reagent Co., Ltd., (China). All chemicals were of analytical grade without further purification. Milli-Q water obtained from a Millipore system (Millipore, Bedford, MA, USA) was used throughout the experiments. The stock solution of atrazine (1,000 mg/L) was prepared by dissolving 0.100 g atrazine in 0.100 L methanol and stored at 4°C. The individual working solutions of atrazine (1, 2, 5, 8, 10, 15, 20, 25, and 30 mg/L) were prepared by diluting the corresponding stock solution with Milli-Q water.

2.2. Synthesis of GPC

GO was prepared using a modified Hummer' method [36]. GO was dispersed in Milli-Q water and sonicated in

an ultrasound bath for 2 h. The sonicated dispersion was then processed by freeze-drying for 24 h.

The synthesis of GPC was described as follows: first, GO powders were irradiated in a domestic microwave oven (Galanz, P70D20P-N9, China) operated at high power (700 W) for 1.5 min. During the irradiation, a large volume expansion of the GO powder occurred and the black, fluffy microwave exfoliated graphite oxide powder was collected. Second, 800 mg of the obtained powder was dispersed in 40 mL 7 M aqueous KOH solution and stirred for 4 h at a speed of 400 rpm, followed by another 24 h of static soaking in ambient conditions. The extra KOH solution was removed by filtering the mixture through a PTFE filtration membrane (Jinteng, 0.45 μm); then the mixture was dried in the lab oven at 65°C for 24 h. The dry mixture was placed in a Nickel boat and heated at 800°C for 1 h in a horizontal tube furnace (50 mm diameter), with a nitrogen flow of 120 sccm. The temperature was ramped from room temperature to 800°C at 5°C 1/min. After cooling down in vacuum, the sample was repeatedly washed by de-ionized water until a pH value of 7 was reached. Then the sample was dried at 65°C in ambient for 2 h to generate GPC powders.

2.3. Sample characterization

The microstructure and morphology of the samples were analyzed by scanning electron microscopy (SEM) (JSM-6400-SEM, JEOL, Japan) with an accelerating voltage of 5 kV. Measurement of the nitrogen adsorption isotherms was done with a NOVA 2000 sorptometer (Quantachrome instruments, USA) at 77.4 K. The samples were outgassed at 150°C for 16 h under turbomolecular vacuum pumping prior to the gas adsorption measurements. The total surface area and pore volume were calculated with the Brunauer–Emmett–Teller (BET) method. The pore size distributions were evaluated with the Barrett–Joyner–Halenda (BJH) method.

Fourier transform infrared (FT-IR) spectra were recorded using a Thermo Nicolet 6700 FTIR spectrometer (Thermo Fisher, America) that was equipped with a TGS/PE detector and a silicon beam splitter with 4 cm⁻¹ resolution. The sample disks were prepared by mixing oven-dried (at 105°C) samples with spectroscopy-grade potassium bromide in an agate mortar. FTIR spectra were obtained in the range of 500–4,000 cm⁻¹. Powder X-ray diffractometer (X'Pert Pro, PANalytical, Netherland) equipped with a copper anode generating Cu Kα radiation ($k = 1.5406 \text{ \AA}$) was used to investigate the crystal structure of these sorbents. X-ray diffraction (XRD) analysis were carried out from 5° to 50° in 2θ using an 8 s counting time and a stepping rate of 0.04 1/min at room temperature. Raman spectra were recorded on a microscope Raman spectrometer (Thermo Fisher Scientific, USA) with a 532 nm laser.

2.4. Batch sorption experiments

The adsorption properties of atrazine by GO and GPC were determined in batch experiments. Briefly, 60 mL atrazine solution and 3 mg sorbent samples were placed in a 100 mL glass bottle. The pH of the solution was adjusted

to 6.0 ± 0.1 with 0.1 M NaOH or HCl solutions. Sample bottles were shaken on a shaker (HZQ-X500C, Shanghai Yiheng Scientific Instrument Co., Ltd., China) at $25^\circ\text{C} \pm 0.1^\circ\text{C}$ and a rate of 200 rpm. For kinetic experiments, 1 mL sample was taken out at 0.5, 1, 2, 4, 8, 20, 60, 180, and 360 min from different bottles for analysis of atrazine concentration. Sorption isotherms were determined by mixing 3 mg sorbent samples with 60 mL atrazine solution at an initial concentration ranging from 1 to 30 mg/L and shaken for 48 h. The effect of ionic strength on atrazine adsorption was examined in 30 mg/L atrazine solution with varying concentrations (0.1, 0.2, 0.3, and 0.4 M) of NaCl solution. The effect of solution pH on atrazine removal was studied in the range of 2–10 with 30 mg/L atrazine solutions. The initial pH values of all the solutions were adjusted using 0.1 mol/L HCl or 0.1 mol/L NaOH solutions with desired concentrations. All adsorption experiments were conducted in triplicate, and the mean values and deviations were reported.

After being centrifuged, the supernatant of each sample was filtered through 0.45 μm filter and analyzed. Atrazine concentration was determined according to the absorbance at the wavelength of 222 nm by a UV-vis spectrometer (UV3600, Shimadzu, Japan). The chemical structure and properties of atrazine were shown in Table 1. A calibration curve was plotted between the absorbance and concentration of atrazine to obtain its absorbance-concentration profile basing on Beer–Lambert's law. For a high concentration of atrazine, it was diluted before absorbance measurement. The concentration of atrazine of the sample was determined by the Beer–Lambert's law expression.

The adsorption capacities of atrazine onto GO and GPC were calculated using the following equation:

$$q_e = \frac{(C_0 - C_e)}{W} \times V \quad (1)$$

where q_e (mg/g) is the adsorption amount of pollutant at equilibrium; C_0 and C_e (mg/L) are the initial and equilibrium pollutant concentrations in solution, respectively; V is the volume of adsorbed solution (L) and W is the mass of adsorbent (g). In the adsorption kinetic experiment, the adsorption amount can be calculated using the following equation:

$$q_t = \frac{(C_0 - C_t)}{W} \times V \quad (2)$$

where q_t (mg/g) is the adsorbed amount of pollutant at time of t (min). C_t (mg/L) is the residual concentrations of pollutants in the solution at the time of t .

3. Results and discussion

3.1. Characterization of GO and GPC

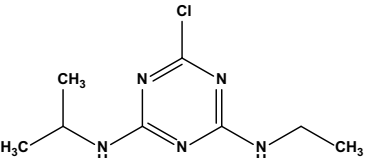
SEM technique was used to study the surface morphological features of the adsorbents. The micrographs in Fig. 1 presented the SEM profiles of GO and GPC. The image of GO showed that GO was in the form of flexible sheets with many wrinkles. However, the surface morphology of GPC exhibited a large number of widened pores with cracks and agglomerations by KOH. The porous structure of GPC was not homogenous and irregular pores with different shapes and sizes were observed. The destruction of graphite structure and increase of pores are beneficial for the molecular diffusion into the inner pore systems, providing more interfaces for adsorption.

EDX was used to qualitatively analyze the elements of the two materials as shown in Fig. 1. It can be seen clearly that the content of oxygen on the surface of GPC reduced sharply from 41.06% to 8.08%, indicating the increase of hydrophobicity and aromaticity and the reduction of polar groups. Simultaneously, 3.49% potassium had been doped into GPC.

Fig. 2a illustrates the nitrogen adsorption/desorption isotherms of GO and GPC. The pore size distributions (shown in Fig. 2b) calculated by BJH method showed main pore sizes around 2–50 nm for GPC. The BET surface area of GPC were 1,598 m^2/g , which was more than ten times higher than those of GO of 15 m^2/g . Compared to the one-step KOH activation method as described in the work of Guo et al. [28], the BET surface area of GPC was increased by almost 1.5 times. The BJH desorption cumulative pore volume of GPC was 0.64 cm^3/g , much higher than that of GO of 0.041 cm^3/g . The results indicated that the combination of microwave exfoliation and alkali treatment was a high-efficiency technique for producing a large amount of porous structures, which was also confirmed by SEM images.

The functional groups are closely related to the specific chemical properties, which affect its adsorption capacity. FT-IR was performed to identify the functional groups and the spectrum is shown in Fig. 3. The characteristic bands at near $3,448 \text{ cm}^{-1}$ were attributed to the –OH stretching

Table 1
General data of atrazine used in this work

Chemical construction	Formula	Molecular weight (g/mol)	λ_{max}^a (nm)	Solubility ^b (mg/L)
	$\text{C}_8\text{H}_{14}\text{ClN}_5$	215.72	222	34.5

^aDetermined by UV-vis spectrometer UV-3600 over a range from 190 to 1,000 nm.

^bIn pure water medium at 25°C .

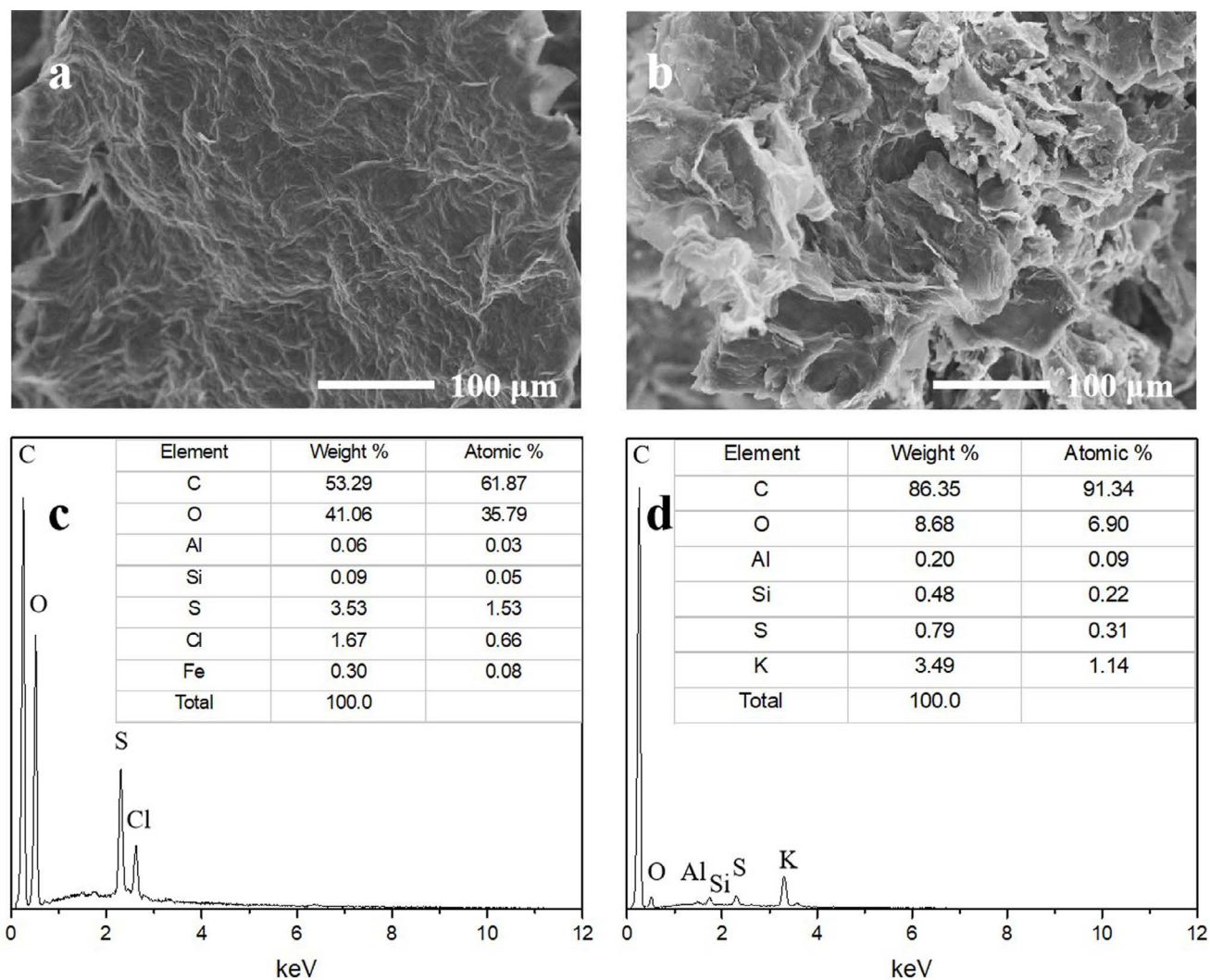


Fig. 1. SEM images and EDX analysis of GO (a and c) and GPC (b and d).

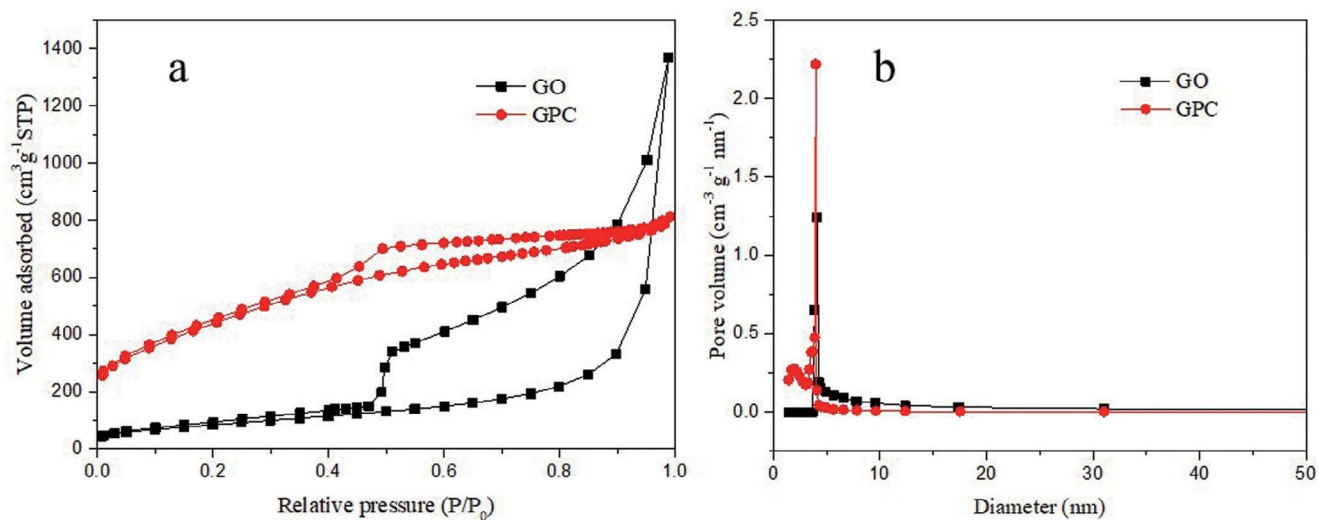


Fig. 2. N₂ adsorption/desorption isotherms (a) and pore size distributions (b) of GO and GPC.

vibrations arising from –OH group in both GO and GPC. The peaks including C=O ($1,583\text{ cm}^{-1}$) skeletal vibration and C=C ($1,623\text{ cm}^{-1}$) stretching vibration from carbonyl and carboxyl groups remained after microwave and KOH treatment. The peaks at about $1,106\text{ cm}^{-1}$ in GPC can be ascribed to the vibration of C–O in the epoxy groups. The microwave treatment process reduced GO which may increase the anchoring sites for atrazine molecules.

As shown in Fig. 4, XRD analysis of GPC displayed diffraction peaks at around $2\theta = 26.6^\circ$, 42.5° , and 44.7° which corresponded to the layer-to-layer distance (d -spacing) of about 0.33 nm (d_{002}), 0.21 nm ($d_{100'}$, not obvious), and 0.20 nm ($d_{101'}$, not obvious). The diffraction peaks of GO were found at approximately $2\theta = 9.5^\circ$ and 41.9° corresponding to the d -spacing of about 0.93 nm (d_{001}) and 0.22 nm (d_{100}), respectively. Compared to GO, the d -spacing of GPC was reduced

significantly which indicated that some oxygen-containing functional groups were removed. Besides, the crystalline size of GPC was much smaller than that of GO as shown by the lower X-ray peak of GPC. It indicated that GPC had more structure defects, endowing GPC a much higher specific surface area which was favorable for the adsorption of atrazine on the surface of GPC.

Raman spectra (Fig. 5) of GO and GPC showed two prominent peaks at high frequencies. The peak at $1,344\text{ cm}^{-1}$ represented mode D-band induced by defect-related vibration mode, which was due to edge defects, disordered carbon, and other defects. The peak at $1,615\text{ cm}^{-1}$ was ordered mode G-band originated from crystalline graphitic/ sp^2 carbon atoms. The peak intensity ratio of D–G bands (I_D/I_G) is an index for evaluating the defects of graphene material. The I_D/I_G of GPC ($I_D/I_G = 1.04$) was larger than that of GO ($I_D/I_G = 0.85$), reflecting increased defects in GPC. This result

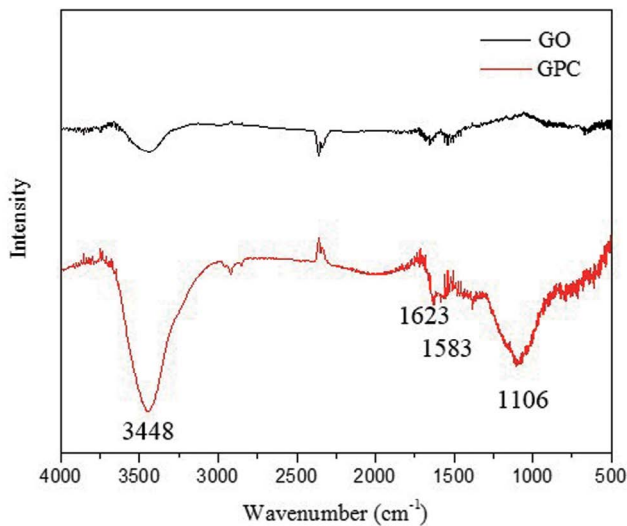


Fig. 3. FTIR spectra of GO and GPC.

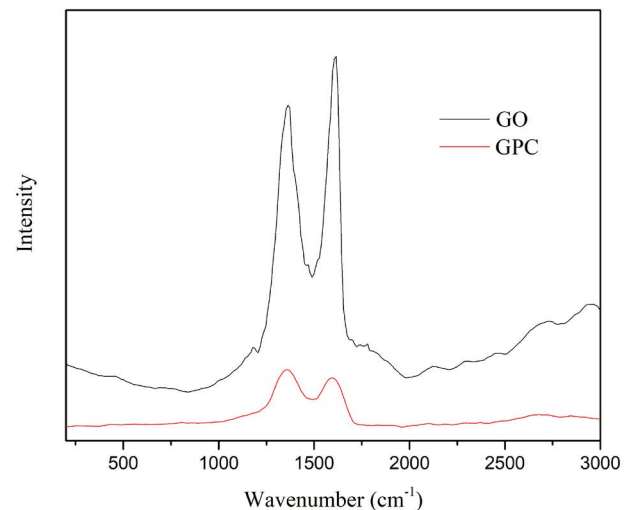


Fig. 5. Raman spectra of GO and GPC.

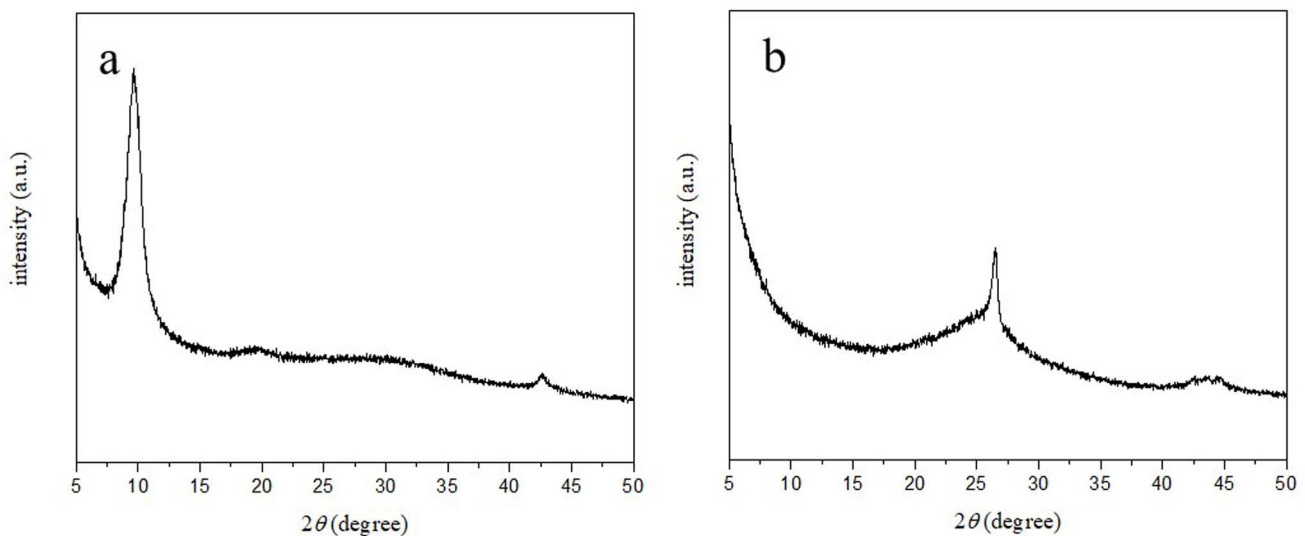


Fig. 4. XRD patterns of GO (a) and GPC (b).

was consistent with SEM and RXD data. Zeta potential of GO and GPC is depicted in Fig. 6. Compared to GO, positive charges increased at the surface of GPC.

3.2. Effects of dosage on atrazine adsorption capacity

The effect of dosage (described as the weight ratio of solid to liquid) is an important factor that may affect adsorption capacity. The effects of the adsorbent dosage on atrazine adsorption capacity are shown in Fig. 7. The results revealed that the adsorption capacity of atrazine decreased with increasing dosage of GPC over the range of 0.05–0.25 g/L. This was due to that the adsorption had reached equilibrium concentration, leaving a large number of effective sites unused. Besides, high GPC dosage may increase the viscosity and inhibit the diffusion of atrazine

molecules to the surface of GPC. As for GO, the adsorbent dosage exhibited no obvious influence on the adsorption capacity. Considering both the cost and adsorption capacity, the adsorbent dosage was selected as 0.05 g/L.

3.3. Adsorption kinetics of atrazine

Sorption kinetics are presented in Fig. 8. The adsorption removal of atrazine on GO and GPC were very fast at the initial period and then became slow with the increase of contact time, reaching equilibrium after ~500 min.

Adsorption is a physiochemical process that involves mass transfer of a solute from the liquid phase to the solid surface. Adsorption kinetic studies are essential for the further perspective for the adsorption mechanisms and characteristics. Hence, mathematical models were used to simulate the kinetics of pollutant adsorption on the sorbents. The pseudo-first-order, pseudo-second-order, intra-particle diffusion (Weber Morris), and Elovich equations were applied to fit experimental data obtained from batch experiments.

$$\ln(q_e - q_t) = \ln q_e - k_1 t \quad (\text{pseudo-first-order}) \quad (3)$$

$$\frac{t}{q_t} = \frac{1}{k_2 q_e^2} + \frac{1}{q_e} t \quad (\text{pseudo-second-order}) \quad (4)$$

$$q_t = k_d \times t^{0.5} + C \quad (\text{intra-particle diffusion}) \quad (5)$$

$$q_t = \frac{1}{\beta} \ln(\alpha\beta) + \frac{1}{\beta} \ln t \quad (\text{Elovich}) \quad (6)$$

where k_1 is the pseudo-first-order adsorption rate coefficient (1/min); k_2 is the pseudo-second-order rate constant (g/mg/min); k_d (g/mg/min^{0.5}) is the intra-particle diffusion rate constant and C is the thickness of the boundary

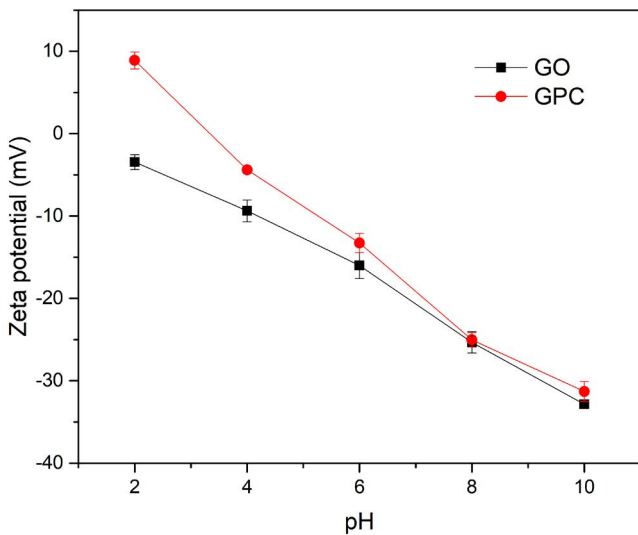


Fig. 6. Zeta potentials of GO and GPC (0.05 M NaNO₃, T = 25°C).

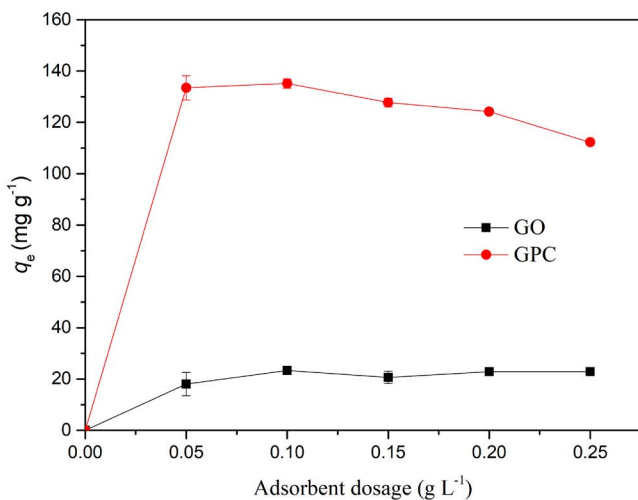


Fig. 7. Effect of adsorbent dosage on the adsorption capacity of atrazine onto GO and GPC ($C_0 = 30$ mg/L, $V = 60$ mL, $T = 298$ K, pH = 6, and contact time $t = 48$ h).

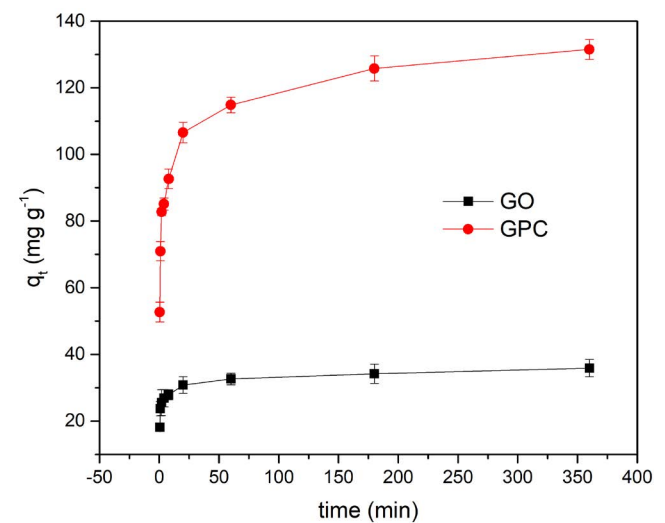


Fig. 8. Kinetics of atrazine sorption onto GO and GPC ($C_0 = 30$ mg/L, $V = 60$ mL, $W = 3$ mg, $T = 298$ K, pH = 6, and contact time $t = 48$ h).

layer (mg/g); Elovich constant α (mg/g/min) and β (mg/g) represent the initial adsorption and desorption coefficient, respectively.

Pseudo-first-order model usually fits well with the predominant adsorption process of physical adsorption. While the pseudo-second-order model is applied when the chemical adsorption is the rate control step. The intra-particle diffusion model is usually used when solute diffusion is considered in the adsorption process, especially for porous materials. Elovich model assumes that heterogeneous adsorption energy distributes on the surface of the adsorbents.

The linear fitting results of the above four models are shown in Fig. 9 and the kinetic calculated kinetic parameters are summarized in Table 2. The R^2 values of the pseudo-second-order model (Fig. 9a) of GPC were much higher than that of pseudo-first-order model (Fig. 9b). The calculated q_e values of pseudo-second-order model of both GO and GPC were close to the experimental ones. The fitting obtained

for the adsorbents indicated that the adsorption conforms to a pseudo-second-order reaction highlighting the chemical adsorption rate-controlling mechanism. Two straight lines in the intra-particle diffusion model are shown in Fig. 9c corresponding to two intra-particle diffusion rate constant k_{d1} and k_{d2} . The values decreased from k_{d1} to k_{d2} and the diffusion rate constant values of GPC were larger than those of GO at the two stages, which were consistent with the data shown in Figs. 7 and 8. The adsorption process can be explained as follows: (1) the first stage corresponded to external mass transfer of atrazine molecules to the adsorbent exterior surface; (2) the second stage attributed to intra-particle diffusion or inner diffusion with gradual equilibrium adsorption. So the overall adsorption process was jointly controlled by external mass transfer and inner diffusion. Besides, the α values were several orders larger than the β values on each fitting plot from Elovich equation as shown in Fig. 9d. The results also confirmed that the adsorption rates of atrazine onto GO and GPC were controlled by chemical adsorption.

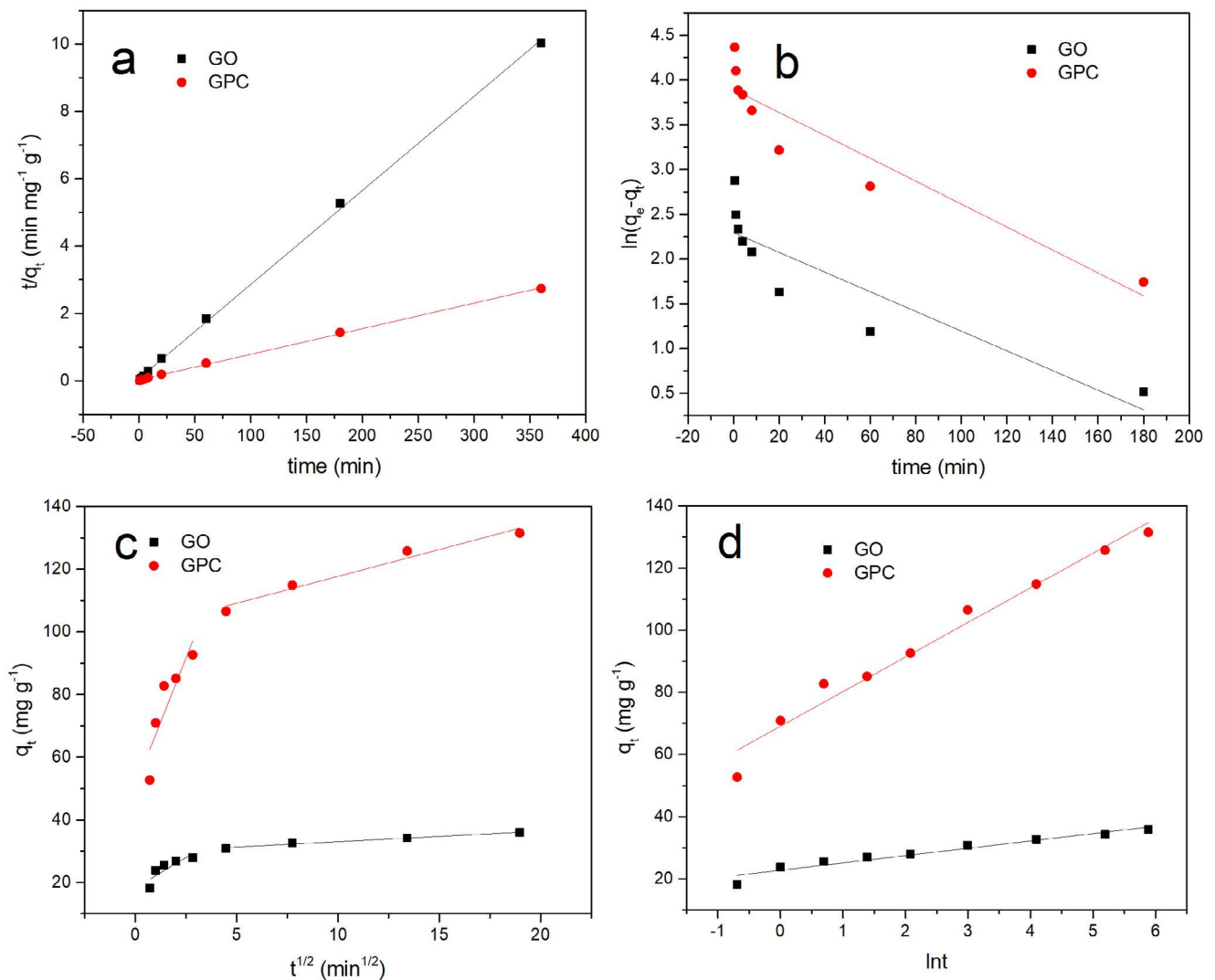


Fig. 9. Pseudo-second-order kinetics (a), pseudo-first-order kinetics (b), intra-particle diffusion kinetics (c), and Elovich kinetics (d) for adsorption of atrazine onto GO and GPC.

3.4. Adsorption isotherms of atrazine

Figs. 10 and 11 show the equilibrium isotherms for adsorption of atrazine onto GO and GPC. Langmuir (Fig. 11a) and Freundlich (Fig. 11b) models were used to analyze the adsorption isotherms of pollutant on the adsorbents. The Langmuir model assumes monolayer sorption onto a homogeneous surface with no interactions between the adsorbed molecules. The Langmuir empirical equation used are given below:

$$\frac{C_e}{q_e} = \frac{C_e}{Q_m} + \frac{1}{K_L Q_m} \quad (7)$$

where q_e (mg/g) is the sorption amount of pollutants at equilibrium, Q_m (mg/g) is the maximum sorption

capacity; K_L (L/g) is the Langmuir constant that related to free energy of sorption.

The Freundlich model is an empirical equation, which is often used to describe chemisorption on heterogeneous surface. The Freundlich isotherm equation is expressed as:

$$\ln q_e = \ln K_F + \frac{1}{n} \ln C_e \quad (8)$$

where K_F ($\text{mg}^{1-n} \text{L}^n/\text{g}$) is the Freundlich constant related to sorption capacity; n is the empirical parameter varying with the degree of heterogeneity of adsorbing sites.

The equilibrium adsorption isotherms were further interpreted following the Langmuir-Freundlich model as shown in Fig. 12:

$$q_e = Q_{\max} \frac{(K_{\text{LF}} C_e)^n}{1 + (K_{\text{LF}} C_e)^n} \quad (9)$$

where K_{LF} is the Langmuir-type equilibrium constant defined by the Van't Hoff equation for a heterogeneous solid, and n is the Freundlich heterogeneity factor (the larger the value, the more heterogeneous the system) [37].

The adsorption constants and correlation coefficients are summarized in Table 3. The Freundlich isotherm model showed a better fitting with adsorption data than the Langmuir isotherm model for GO, indicating that there was multilayer adsorption of atrazine onto GO. Compared to the experimental results, the Langmuir-Freundlich fitting for atrazine adsorption on GO was obviously not ideal, as the calculated q_{\max} was 2.21×10^4 mg/L with standard error of 1.25×10^7 . For GPC, R^2 values of the Langmuir model (0.997) was higher than that of the Freundlich model (0.973) and Langmuir-Freundlich model (0.954), suggesting monolayer sorption onto a homogeneous surface. The maximum sorption capacity of the adsorbents obtained from Langmuir model was 133.5 mg/g for GPC. The large K_L values of the

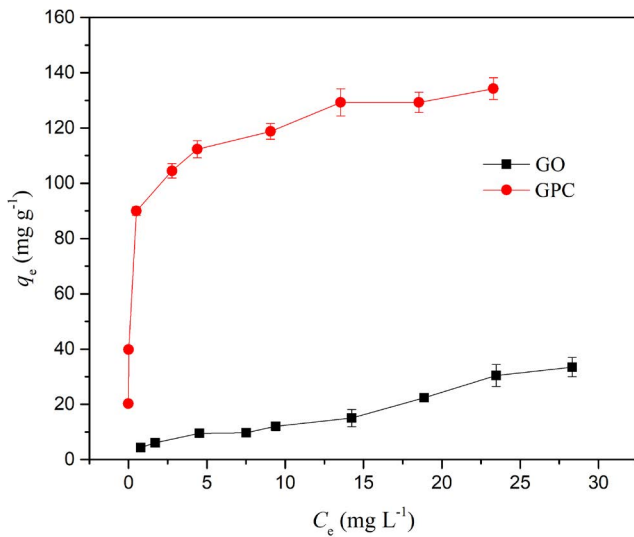


Fig. 10. Equilibrium adsorption isotherms of atrazine on GO and GPC ($V = 60$ mL, $W = 3$ mg, $T = 298$ K, $\text{pH} = 6$, and contact time $t = 48$ h).

Table 2
Parameters for the four kinetic models of atrazine adsorption

Adsorbent	Pseudo-first-order				Pseudo-second-order		
	$q_{e,\text{exp}}$ (mg/g)	$q_{e,\text{cal}}$ (mg/g)	k_1 (1/min)	R^2	$q_{e,\text{cal}}$ (mg/g)	$k_2 \times 10^{-3}$ (g/mg/min)	R^2
GO	35.9	9.91	0.011	0.758	35.8	0.012	0.999
GPC	131.5	49.1	0.013	0.861	131.4	0.0023	0.999
Adsorbent	Intra-particle diffusion						
	k_{d1} (g/mg/min ^{0.5})	C_1 (mg/g)	R_1^2	k_{d2} (g/mg/min ^{0.5})	C_2 (mg/g)	R_2^2	
GO	3.86	18.30	0.626	0.338	29.61	0.971	
GPC	16.35	50.84	0.715	1.716	100.54	0.955	
Adsorbent	Elovich kinetics						
	α (mg/g/min)	β (mg/g)	R^2				
GO	3.61×10^4	0.424	0.936				
GPC	5.49×10^3	0.090	0.970				

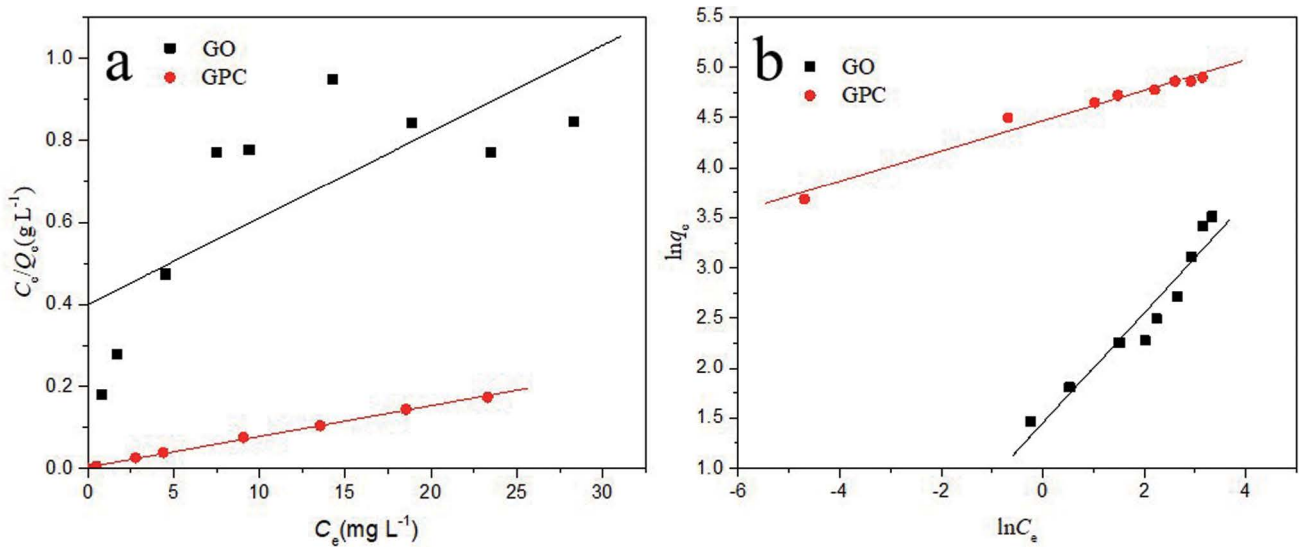


Fig. 11. Langmuir (a) and Freundlich (b) isotherms for the adsorption of atrazine onto GO and GPC.

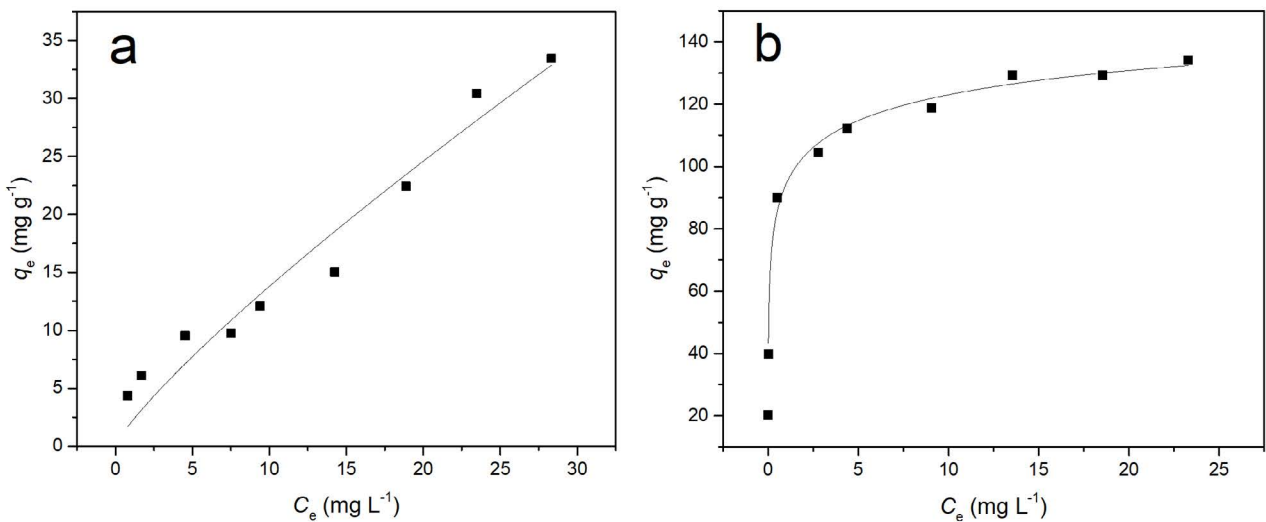


Fig. 12. Experimental data and model fittings of the Langmuir–Freundlich isotherms for the adsorption of atrazine onto GO (a) and GPC (b).

Table 3
Adsorption isotherm parameters for atrazine adsorption onto GO and GPC at 298 K

Adsorbent	Langmuir			Freundlich			Langmuir–Freundlich			
	Q_m (mg/g)	K_L (mg/L)	R^2	$1/n$	K_f (mg $^{1-n}$ L n /g)	R^2	Q_m (mg/g)	K_{LF} (dm 3 /mg)	n	R^2
GO	47.6	0.053	0.566	0.550	4.26	0.926	2.21×10^4	1.51×10^{-5}	0.84	0.915
GPC	133.5	2.31	0.997	0.151	91.4	0.973	187.4	1.06	0.27	0.954

Langmuir model also indicated that atrazine was facile to be adsorbed on to GPC.

We compared the adsorption capacities of atrazine onto different adsorbents. Except for hemp stem-based activated carbons with different surface chemistry, the higher

adsorption capacity surpassed the adsorption performance of many materials as shown in Table 4 [37–43]. The results showed that the combination of chemical and physical treatment method was highly effective for enhancing pollutant adsorption. This proposes a potential of expanding this

Table 4
Comparison of the adsorption capacities of atrazine onto different adsorbents

Adsorbents	BET (m ² /g)	Q _m (mg/g)	References
GPC	1,598	133.5	This work
Biochar	32.85	1.94	[32]
Activated carbon from biochar	466.37	92.23	[32]
Activated carbon HAC	2,135	437	[37]
Activated carbon F400	–	39.37	[38]
Magnetic multi-walled carbon nanotube	138.66	40.16	[39]
Zeolite X	–	11.86	[41]
Heat-treated kerolite	224	15.2	[42]
Activated carbon/iron oxide	568	22	[43]

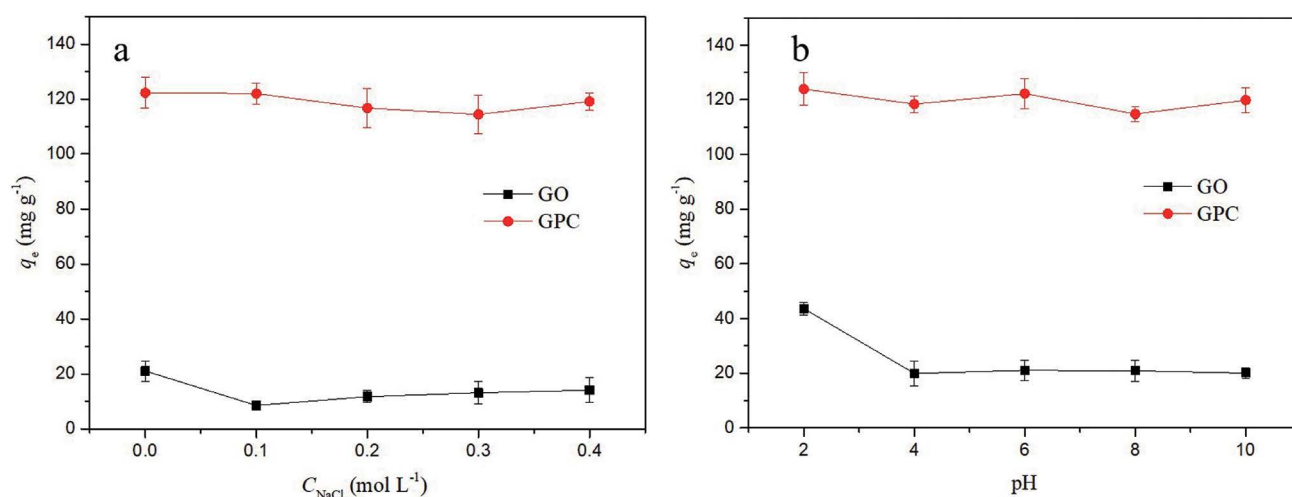


Fig. 13. Effect of ionic strength (a) and pH (b) on the adsorption capacity of atrazine onto GO and GPC ($C_0 = 30$ mg/L, $V = 30$ mL, $W = 3$ mg, $T = 298$ K, and contact time $t = 48$ h).

novel, facile, and low cost technology to produce porous carbon material from other carbon-rich source such as biochar and agricultural or forest residues.

3.5. Effects of ionic strength and pH on the adsorption of atrazine

Fig. 13a shows the adsorption capacity of atrazine on GO and GPC under different ionic strength (0–0.4 M). As the ionic strength was increased from 0 to 0.4 M, the adsorption capacity of GO decreased first and then became unchanged. The ionic strength displayed no significant effect on the adsorption capacity of GPC.

Solution pH not only affects the structure and ionization degree of molecules, but also the functional groups and the surface charges of the adsorbent. Thus, pH is an important factor to affect the adsorption process and capacity. Fig. 13b depicts the adsorption capacities of GO and GPC in the pH range of 2–10. The results showed that the adsorption capacity of GO decreased with the increase of pH when $\text{pH} < 4$. At $\text{pH} > 4$, the adsorption capacity was barely influenced by pH. Besides, the influence of pH on the adsorption capacity of GPC was not obvious at pH from 2 to 10. The $-\text{NH}-$ group can react with protons to the positively

charged form $-\text{NH}_2^+$ at lower pH, which was favorable for the adsorption onto negatively charged GO due to electrostatic reaction. Higher the pH of the solution was, higher the repulsion between the adsorbents and atrazine molecules was, leading to lower adsorption capacity of GO.

Generally, the influence of pH and ionic strength on adsorption capacity for atrazine with GPC is not notable, endowing it a promising application potential under wide pH and ionic strength range.

3.6. Adsorption mechanism of atrazine on to the adsorbents

Previous studies have demonstrated that atrazine can form strong $\pi-\pi$ electron interactions with activated biochar [33]. $\pi-\pi$ interactions is one of the driving forces for the adsorption of organic pollutants with benzene rings onto graphene material [41]. Due to the electronegative N atoms incorporated into the ring and the $-\text{Cl}$ substituent which is electron withdrawing, atrazine molecule is π -electron deficient. The polyaromatic surface of GPC are π -electron rich [33,42–45]. The enhanced adsorption of atrazine can be mainly attributed to the strong interactions between atrazine molecules and GPC through $\pi-\pi$ electron donor–acceptor

force. Thus, The GPC can be also applied as an effective and low-cost adsorbent to remove other aromatic pollutants from water.

Hydrogen bond widely exists in the process of polar organic pollutant sorption on carbon nanomaterials. The negatively charged groups of hydroxyl (–OH) and carboxyl (–COOH) available on GPC can form hydrogen bonds with *N* atoms of atrazine ring. Besides, the largely increased surface area and pore volume may play a vital role in the adsorption process, endowing the adsorbent a lot of active sites for physical adsorption.

4. Conclusion

The GPC with highly enhanced adsorption performance has been prepared by a combined strategy of microwave exfoliation and high temperature KOH activation. The synthesized carbon nanomaterial showed excellent adsorption capacity, which was increased by almost two times compared to pristine GO. The results indicated that GPC was a promising sorbent for atrazine removal due to its extremely high BET surface area. Findings of this study open new possibilities in producing innovative and effective engineered porous carbon nanomaterials for water purification and other various environmental applications in the future.

Acknowledgments

We gratefully acknowledge the financial support from the National Natural Science Foundation of China (No. 21707003) and the Science and Technology Planning Project of Shenzhen municipality, China (JCYJ 2015062914 4818001). We also appreciate anonymous reviewers for their valuable comments to improve this manuscript.

References

- [1] National Academy of Engineering, Grand Challenges, 2014. Available at: <http://www.engineeringchallenges.org/cms/challenges.aspx>
- [2] P. Short, T. Colborn, Pesticide use in the US and policy implications: a focus on herbicides, *Toxicol. Ind. Health*, 15 (1999) 240–275.
- [3] K. Sun, B. Gao, Z.Y. Zhang, G.X. Zhang, Y. Zhao, B.S. Xing, Sorption of atrazine and phenanthrene by organic matter fractions in soil and sediment, *Environ. Pollut.*, 158 (2010) 3520–3526.
- [4] K. Muir, S. Rattanamongkolgul, M. Smallman-Raynor, M. Thomas, S. Downer, C. Jenkinson, Breast cancer incidence and its possible spatial association with pesticide application in two counties of England, *Public Health*, 118 (2004) 513–520.
- [5] J.P. Lasserre, F. Fack, D. Revets, S. Planchon, J. Renaut, L. Hoffmann, A.C. Gutleb, C.P. Muller, T. Bohn, Effects of the endocrine disruptors atrazine and PCB 153 on the protein expression of MCF-7 human cells, *J. Proteome Res.*, 8 (2009) 5485–5496.
- [6] T.A. Fouladi, T. Kaghazchi, M. Soleimani, Adsorption of cadmium from aqueous solutions on sulfurized activated carbon prepared from nut shells, *J. Hazard. Mater.*, 165 (2009) 1159–1164.
- [7] L.F. Delgado, P. Charles, K. Glucina, C. Morlay, Adsorption of ibuprofen and atenolol at trace concentration on activated carbon, *Sep. Sci. Technol.*, 50 (2015) 1487–1496.
- [8] F. Hayeeye, M. Sattar, W. Chinpa, O. Sirichote, Kinetics and thermodynamics of Rhodamine B adsorption by gelatin/activated carbon composite beads, *Colloids Surf., A*, 513 (2017) 259–266.
- [9] H.W. Luo, W.W. Law, Y.C. Wu, W.P. Zhu, E.-H. Yang, Hydrothermal synthesis of needle-like nanocrystalline zeolites from metakaolin and their applications for efficient removal of organic pollutants and heavy metals, *Microporous Mesoporous Mater.*, 272 (2018) 8–15.
- [10] V. Jabbari, J.M. Veleta, M. Zarei-Chaleshtori, J. Gardea-Torresdey, D. Villagran, Green synthesis of magnetic MOF@GO and MOF@CNT hybrid nanocomposites with high adsorption capacity towards organic pollutants, *Chem. Eng. J.*, 304 (2016) 774–783.
- [11] B.N. Bhadra, S.H. Jhung, Adsorptive removal of wide range of pharmaceuticals and personal care products from water using bio-MOF-1 derived porous carbon, *Microporous Mesoporous Mater.*, 270 (2018) 102–108.
- [12] I. Ahmed, S.H. Jhung, Adsorptive desulfurization and denitrogenation using metal organic frameworks, *J. Hazard. Mater.*, 301 (2016) 259–276.
- [13] C. Wang, X. Liu, N.K. Demir, J.P. Chen, K. Li, Applications of water stable metal organic frameworks, *Chem. Soc. Rev.*, 45 (2016) 5107–5134.
- [14] G. Singh, K.S. Lakhi, K. Ramadass, S. Kim, D. Stockdale, A. Vinu, A combined strategy of acid-assisted polymerization and solid state activation to synthesize functionalized nanoporous activated biocarbons from biomass for CO₂ capture, *Microporous Mesoporous Mater.*, 271 (2018) 23–32.
- [15] A.T. Xie, J.D. Dai, X. Chen, Ultrahigh adsorption of typical antibiotics onto novel hierarchical porous carbons derived from renewable lignin via halloysite nanotubes-template and *in-situ* activation, *Chem. Eng. J.*, 304 (2016) 609–620.
- [16] B.L. Chen, Z.X. Yang, G.P. Ma, Heteroatom-doped porous carbons with enhanced carbon dioxide uptake and excellent methylene blue adsorption capacities, *Microporous Mesoporous Mater.*, 257 (2018) 1–8.
- [17] Q.R. Guo, C. Chong, L.J. Zhou, Design of ZIF-8/ion copolymer hierarchically porous material: coordination effect on the adsorption and diffusion for carbon dioxide, *Microporous Mesoporous Mater.*, 261 (2018) 79–87.
- [18] M.R. Benzigar, S.N. Talapaneni, S. Joseph, K. Ramadass, G. Singh, J. Scaranto, U. Ravon, K. Al-Bahily, A. Vinu, Recent advances in functionalized micro and mesoporous carbon materials: synthesis and applications, *Chem. Soc. Rev.*, 47 (2018) 2680–2721.
- [19] S.W.L. Ng, G. Yilmaz, W.L. Ong, G.W. Ho, One-step activation towards spontaneous etching of hollow and hierarchical porous carbon nanospheres for enhanced pollutant adsorption and energy storage, *Appl. Catal., B*, 220 (2018) 533–541.
- [20] W. Chaikittisilp, K. Ariga, Y. Yamauchi, A new family of carbon materials: synthesis of MOF derived nanoporous carbons and their promising applications, *J. Mater. Chem. A*, 1 (2013) 14–19.
- [21] A.K. Geim, K.S. Novoselov, The rise of graphene, *Nat. Mater.*, 6 (2007) 183–191.
- [22] Y. Zhu, S. Murali, W. Cai, X. Li, W.S. Ji, Graphene and graphene oxide: synthesis, properties, and applications, *Adv. Mater.*, 22 (2010) 3906–3924.
- [23] M. Segal, Selling graphene by the ton, *Nat. Nanotechnol.*, 4 (2009) 612–614.
- [24] Y. Shen, Q.L. Fang, B.L. Chen, Environmental applications of three-dimensional graphene-based macrostructures: adsorption, transformation, and detection, *Environ. Sci. Technol.*, 49 (2015) 67–84.
- [25] J. Zhao, Z.Y. Wang, J.C. White, B.S. Xing, Graphene in the aquatic environment: adsorption, dispersion, toxicity and transformation, *Environ. Sci. Technol.*, 48 (2014) 9995–10009.
- [26] D.R. Dreyer, S. Park, C.W. Bielawski, R.S. Ruoff, The chemistry of graphene oxide, *Chem. Soc. Rev.*, 39 (2010) 228–240.
- [27] L.H. Jiang, Y.G. Liu, G.M. Zeng, F.Y. Xiao, X.J. Hu, X. Hu, H. Wang, T.T. Li, L. Zhou, Removal of 17 beta-estradiol by few layered graphene oxide nanosheets from aqueous solutions: external influence and adsorption mechanism, *Chem. Eng. J.*, 284 (2016) 93–102.

- [28] Y.F. Guo, J. Deng, J.Y. Zhu, C.Y. Zhou, X.J. Zhou, R.B. Bai, Removal of anionic azo dye from water with activated graphene oxide: kinetic, equilibrium and thermodynamic modeling, *RSC Adv.*, 6 (2016) 39762–39773.
- [29] W.C. Peng, S.Z. Liu, H.Q. Sun, Y.J. Yao, L.J. Zhi, S.B. Wang, Synthesis of porous reduced graphene oxide as metal-free carbon for adsorption and catalytic oxidation of organics in water, *J. Mater. Chem. A*, 1 (2013) 5854–5859.
- [30] Y.H. Zhang, Y.L. Tang, S.Y. Li, Sorption and removal of tetrabromobisphenol A from solution by graphene oxide, *Chem. Eng. J.*, 222 (2013) 94–100.
- [31] F. Yang, L.L. Sun, W. Zhang, Y. Zhang, One-pot synthesis of porous carbon foam derived from corn straw: atrazine adsorption equilibrium and kinetics, *Environ. Sci.: Nano*, 4 (2017) 625–635.
- [32] G.C. Tan, W.L. Sun, Y.R. Xu, H.Y. Wang, N. Xu, Sorption of mercury(II) and atrazine by biochar, modified biochars and biochar based activated carbon in aqueous solution, *Bioresour. Technol.*, 211 (2016) 727–735.
- [33] Y.W. Zhu, S. Murali, M.D. Stoller, K.J. Ganesh, W.W. Cai, P.J. Ferreira, A. Pirkle, R.M. Wallace, K.A. Cychoz, M. Thomas, D. Su, E.A. Stach, R.S. Ruoff, Carbon-based supercapacitors produced by activation of graphene, *Science*, 332 (2011) 1537–1541.
- [34] H.M.A. Hassan, V. Abdelsayed, A.E.R.S. Khder, K.M. Abouzeid, J. Ternner, M.S. El-Shall, S.I. Al-Resayes, A.A. El-Azhary, Microwave synthesis of graphene sheets supporting metal nanocrystals in aqueous and organic media, *J. Mater. Chem.*, 19 (2009) 3832–3837.
- [35] Y.W. Zhu, S. Murali, M.D. Stoller, A. Velamakanni, R.D. Piner, R.S. Ruoff, Microwave assisted exfoliation and reduction of graphite oxide for ultracapacitors, *Carbon*, 48 (2010) 2106–2122.
- [36] W.S. Hummers, R.E. Offeman, Preparation of graphitic oxide, *J. Am. Chem. Soc.*, 80 (1958) 1339–1342.
- [37] I. Lupul, J. Yperman, R. Carleer, G. Gryglewicz, Adsorption of atrazine on hemp stem-based activated carbons with different surface chemistry, *Adsorption*, 21 (2015) 489–498.
- [38] P. Chingombe, B. Saha, R.J. Wakeman, Sorption of atrazine on conventional and surface modified activated carbons, *J. Colloid Interface Sci.*, 302 (2006) 408–416.
- [39] W.W. Tang, G.M. Zeng, J.L. Gong, Y. Liu, X.Y. Wang, Y.Y. Liu, Z.F. Liu, L. Chen, X.R. Zhang, D.Z. Tu, Simultaneous adsorption of atrazine and Cu(II) from wastewater by magnetic multi-walled carbon nanotube, *Chem. Eng. J.*, 211–212 (2012) 470–478.
- [40] C. Pelekani, V.L. Snoeyink, A kinetic and equilibrium study of competitive adsorption between atrazine and Congo red dye on activated carbon: the importance of pore size distribution, *Carbon*, 39 (2001) 35–37.
- [41] T.S. Jamil, T.A. Gad-Allah, H.S. Ibrahim, T.S. Saleh, Adsorption and isothermal models of atrazine by zeolite prepared from Egyptian kaolin, *Solid State Sci.*, 13 (2011) 198–203.
- [42] M.D. Ureña-Amate, M. Socías-Viciana, E. González-Pradas, M. Saifi, Effects of ionic strength and temperature on adsorption of atrazine by a heat treated kerolite, *Chemosphere*, 59 (2005) 69–74.
- [43] C.S. Castro, M.C. Guerreiro, M. Gonçalves, L.C.A. Oliveira, A.S. Anastácio, Activated carbon/iron oxide composites for the removal of atrazine from aqueous medium, *J. Hazard. Mater.*, 164 (2009) 609–614.
- [44] F. Xiao, J.J. Pignatello, Interactions of triazine herbicides with biochar: steric and electronic effects, *Water Res.*, 80 (2015) 179–188.
- [45] A. Rochefort, J.D. Wuest, Interaction of substituted aromatic compounds with graphene, *Langmuir*, 25 (2009) 210–215.